UNIVERSITY OF PARDUBICE
FACULTY OF TRANSPORT ENGINEERING

Dynamic Fracture Behaviour of High Strength Steels

DOCTORAL DISSERTATION
(ANNOTATION)

2018 Ing. Fatih Bozkurt

Doctorand: Ing. Fatih Bozkurt

Programme of Study:
P3710 Technique and Technology in Transport and Communications

Branch of study:
3706V005 Transport Means and Infrastructure

Dissertation Title: Dynamic Fracture Behaviour of High Strength Steels

Supervisor: Prof. Ing. Eva Schmidová, Ph.D.

The doctoral dissertation has arisen at the supervising:
Educational and Research Centre in Transport (ERCT)

Abstract

In accordance with the current trend towards the lightweight railway transport means, this dissertation work is focused on the use of advanced high-strength steels. Their mechanical response is based on specific material and technology processes. In this dissertation work, the experimental analyzes of fracture behavior in connection with structural evaluation were conducted. The plane strain fracture toughness (K_{IC}) of Strenx 700MC steel compared to standardly used S355 steel in rail vehicles were determined with two different nonstandardized test methods. The new methodology for evaluation of dynamic response at different loading rates near to crash conditions was used and validated in the experimental part of the work. In order to specify the dynamic fracture toughness (K_{Id}) value, uniaxial impact tensile tests and three-point dynamic fracture tests were performed and evaluated with emphasis on crack propagation mode. Vehicle crashworthiness of high strength steel is greatly influenced by the welded joints because of high energy input during welding. The microstructural changes during the experimental welding process were analyzed and hardness measurements were performed. According to identified critical changes and considering used welding parameters, the weld thermal cycle simulation was applied to Strenx 700MC specimen to evaluate the effect of heat input on fracture behaviour at static and dynamic loading conditions. Lastly, in order to find out the fracture mode depending loading conditions of tested steels, fractography analysis was performed using scanning electron microscopy (SEM).

Keywords

Fracture mechanics, plane strain fracture toughness, dynamic fracture toughness, impact tensile test, fatigue crack growth rate, high strength steel, railway, rail vehicle.

Table of Contents

1. Introduction

Rail transport has been vital issue to the humanity over the centuries, it has shaped the transportation system from past to now and it will definitely shape the future. It covers heavy rail, light rail, tram, funicular and monorail means. They provide numerous advantages, varying from economic to social and energetic to environmental, which makes rail transport the best land transportation option for passengers and freight. When we look at the railway sector for the

transport of passengers and freight, there is an increasing use of this mode in almost every country due to the safety, rapidity, cost effectiveness and environmentally friendly. The growth in the field of rail transport is expected to be doubled in the next decade by considering economic growth in fast developing countries including China, India and Turkey [1].

Rail vehicles are relatively heavy in comparison to other transportation modes. There is a competition among transport industry, especially in rail vehicle manufacturers and operators. They are constantly looking for ways to increase payload and improve energy efficiency. Freight wagons and passenger carriages need to become lighter without compromising on performance, safety and service life. This is possible by examining and improving the design of rail vehicles. The most common procedure is using advanced high strength steel (AHSS) with thinner dimensions [2–9]. It improves the final product and it brings benefits along the way. Experience in using AHSS in other transport sector shows that doubling the strength of the steel can lead to weight reductions of about 30% for up-graded parts [10]. Another important advantage of AHSS is having good energy absorption properties. The crashworthiness of rail cars has been substantially improved by using AHSS [11].

The application of welding process in the production of rail transportation vehicles is essential for structural parts. Many metallurgical changes that take place in the welded area because of high heat input. The region outside the welded joint which is thermally affected by the welding process is known as the heat affected zone (HAZ) and it significantly affects the welded steels. The formation of various HAZ sub-zones depends on various factors, e.g., the metallurgical composition of base metal and weld metal, thermal and mechanical treatments before welding and welding procedures [12–14]. But the investigation of the HAZ of real welded joints is not easy because of the narrowness and heterogeneous structure which is formed in the HAZ. The HAZ can be geometrically extended by welding simulation method in order to determine the different microstructures which can be formed in real welded joints. A considerable amount of literature has been published on weldability

investigations using weld thermal cycle simulation for the identification of the microstructure types in the HAZ [15–27]. The change of microstructural and mechanical properties due to the welding process or welding simulation method can be evaluated by material characterization techniques and investigated on fracture mechanics basis. It is important to know that material behavior during its service life. Taking into consideration of the fracture mechanics, the service life of the structural part can be estimated, and precautions can be taken for safety.

2. Objectives of the Doctoral Dissertation

The dissertation aims to contribute the knowledge of advanced high strength steel (AHSS) application for lightweight constructions. It is necessary to understand two main weak points of prospective application:

i. The influence of the welding process: Because of the primary strengthening process (based on thermomechanical treatment), chosen steel is sensitive to heat input in sense of the drop of primary strength.

ii. The sensitivity to imperfection: In direct connection with welding, the safety requirements are based on reliable non-destructive diagnostic. Fracture mechanics approach is necessary for the determination of the sensitivity of stable crack propagation.

The following set of experimental techniques and analyses were carried out in accordance with the objectives of the dissertation:

1. Three kinds of materials were selected for experimental study:

- S355 steel is a referential steel which is commonly used for structural part of railway transport means,
- Strenx 700MC attributes to the prospective high strength steel for lightweight structures,
- Experimental high strength steel (with increased static and dynamic strength in comparison to Strenx 700MC) was used for extending the experimental scope and validation of used methodology for fracture toughness.

Standard tensile tests were performed using all mentioned steels, results were used for the design of parameters for the next study of sensitivity to internal defects under different structural and loading

conditions. Metallography evaluation was focused on S355 steel and Strenx 700MC steel.

2. Using nonstandardized test methodologies, the static and the dynamic fracture toughness of Strenx 700MC steel, and referential S355 steel were compared.

3. In order to assess the effect of loading rate on dynamic fracture toughness, S355 steel and Strenx 700MC steel were tested at two different impact speeds.

4. In order to evaluate the welding process on the crack sensitivity of Strenx 700MC steel, set of experiments and material analyses were applied:

- Experimental welding of Strenx 700MC defined the structural and mechanical degradation,
- The weld simulation of HAZ enabled testing of homogeneous critical sublayer,
- Static and dynamic tests were conducted by the same (CCRB) method.

5. Dynamic fracture toughness of high strength experimental steel was compared by ISO 26843:2015(E) and CCRB test methodologies.

3. Experimental Procedures

3.1. Welding of Strenx 700MC Plates

Because of the application of Strenx 700MC is a prospective material for lightweight construction in railway, only this kind of steel was examined and evaluated after the welding process. All welding parameters for each welding pass are given in Table 3.1. After or before the welding process, no heat treatment process such as stress relieving was carried out.

Table 3.1 Welding parameters of MAG

Welding Pass	U (Voltage)	I (Current)	Travel speed (mm/min)	Energy (KJ/mm)
1	18.5	140	112	1.1
2	18.5	140	81	1.5
3	18.5	140	102	1.2

3.2. Weld Simulation of Strenx 700MC Specimens

Welding simulation was conducted using WTU 315-3 welding equipment. The prepared specimen was heated by electric arc which was transferred with using copper rings were placed on the specimen.

During the welding simulation process, time – temperature (from heating to cooling) was recorded by Omega HH309A four-channel data logger thermometer as shown in Figure 3.1a. Before and after the weld simulation process of the specimen are shown in Figure 3.1b and Figure 3.1c, respectively.

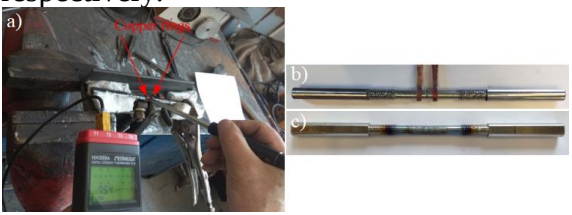

Figure 3.1 a) During the weld simulation process of Strenx 700MC specimen, b) Before weld simulation process of specimen c) After weld simulation process of specimen

3.3. Circumferentially Cracked Round Bar Test Method

The specimen was prepared "V" type notch of 60° with 1 mm radial depth (mean notch radius was 0.225) at the midpoint as shown in Figure 3.2. The important dimensions of the specimen were the diameter of unnotched section (D) was 8 mm, the diameter of notched section (d) was 6 mm, specimen length (L) was 226 mm and gauge length (L_0) was 96 mm.

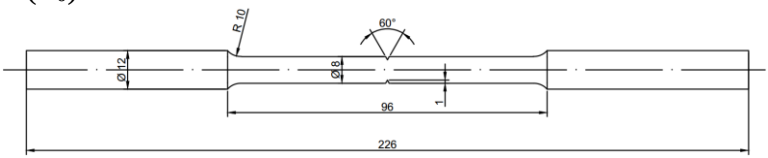

Figure 3.2 Round bar test specimen for CCRB test method

In order to ensure initial fatigue crack in the specimen, R. R. Moore four-point rotating beam fatigue testing machine was used. During the precracking procedure, the specimen was subjected to cyclic tensile – compressive loads of equal amplitude were applied with the stress ratio R_{stress} equal to minus 1 (R_{stress} = -1).

For mode – I loading condition, the precracked specimen was loaded in tension on a universal tensile tester device ZD 10/90. After completion of the uniaxial tests, the fracture surface of the specimen was investigated, and specified dimensions were measured with a stereo optical microscope. For calculation of fracture toughness, defined dimensions were machined notch depth (a_m), length of fatigue

precrack (a_f), crack length due to brittle fracture (a_b) and total crack length (a). The mentioned dimensions were distinct with captured figures as shown in Figure 3.3.

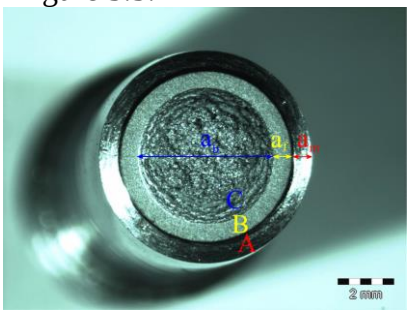

Figure 3.3 Image of the fracture surface of the specimen and defined dimensions

For determination of the fracture toughness of the material, the effective diameter (d_{eff}) was calculated by the sum of machined notch depth and the length of the fatigue precrack as in Equation 3.1

$$d_{eff} = D-2(a_m + a_f) \quad (3.1)$$

Equation 3.1 was used for calculation of fracture toughness as in Equation 3.2 [28],

$$K_{IC}=\frac{P_f}{D^{3/2}}\left[1.72\frac{D}{d_{eff}}-1.27\right] \quad (3.2)$$

where P_f was the maximum fracture load and D was the diameter of the unnotched section. The valid range of Equation 3.2 was $0.46<(d_{eff}/D)<0.86$. For CCRB test method, the fracture toughness of each specimen was calculated according to this proposed equation.

3.4. Determination of Dynamic Fracture Toughness with Nonstandardized Test Method

The methodology of the determination of the dynamic fracture toughness is very similar to CCRB method in terms of material preparation and fatigue precracking procedures. The specimen used for dynamic fracture toughness (K_{Id}) test was threaded round bar which had "V" type notch of 60° with 1 mm radial depth (mean notch radius is 0.225) at the midpoint and it had also M10 thread as shown in Figure 3.4.

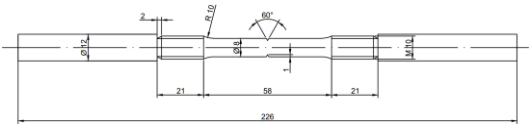

Figure 3.4 The round bar test specimen for dynamic fracture toughness

In present study, Zwick/Roell RKP 450 with PC connected with testXpert testing software was chosen to conduct the instrumented impact tensile testing as shown in Figure 3.5. All tests were conducted at room temperature and during the impact, force – displacement or force – time graph was recorded. In order to investigate the effect of loading rate on the dynamic fracture toughness of the materials, the tests were conducted at two different impact velocities. The first group of material was tested at 5.23 m/s and the second group was tested at 3.48 m/s.

Figure 3.5 a) Pendulum hammer, b) Screwed specimen between tailor block andtup, c) General view of Zwick/Roell RKP 450 pendulum impact tester and d) Anvil

For calculation of dynamic fracture toughness, the defined dimensions were same as in CCRB test method. Depending on the effective diameter (d_{eff}), unnotched section diameter (D) and maximum force (P_{dmax}) during the impact tensile test, dynamic fracture toughness (K_{Id}) was calculated as follow:

$$K_{Id}=\frac{P_{dmax}}{D^{3/2}}\left[1.72\frac{D}{d_{eff}}-1.27\right] \quad (3.3)$$

In the literature, the proposed equation was used only static loading condition to specify the fracture toughness (K_{IC}). This approach provided a novel method to determine the dynamic fracture toughness of the metallic materials using pendulum impact tester.

3.5. Determination of Dynamic Fracture Toughness with Standardized Test Method

It is possible to determine the dynamic fracture toughness of metallic materials using precracked Charpy type test specimen which is explained in ISO 26843:2015(E).

The specimen used for dynamic fracture toughness test was single edge notch bend (SENB or 3-point bending) as shown in Figure 3.6. Precracking was carried out on fatigue testing machine at a constant ΔK level to obtain constant crack growth rate.

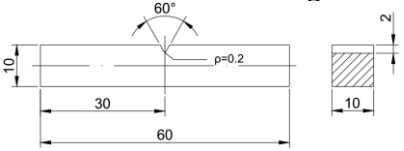

Figure 3.6 Technical drawing of the SENB specimen

In this study, Zwick/Roell RKP 450 by choosing suitable accessories and instrumentation was preferred to conduct the instrumented impact 3-point bending testing. After impact testing, it was necessary to evaluate the force – time curve and the characteristics of this curve was shown in Figure 3.7. First important parameter in this graph was time to fracture (t_f) which was indicated with arrow. Using the measured (t_f), the dynamic fracture toughness K_{Id} was determined as:

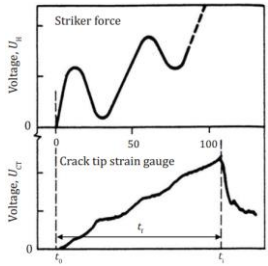

Figure 3.7 Typical force and strain gauge signals during impact

$$K_{Id} = K_I^{dyn}(t=t_f) \quad (3.4)$$

$$K_I^{dyn} = RV_0 f(t') \quad (3.5)$$

where the constant R= 301 GN/m$^{5/2}$, V_0 was impact velocity (5.23 m/s) and the correction factor f(t') was found in Table A1 (in Appendix A) with

$$t' = t\left[1-0.62\left(\frac{a}{W}-0.5\right)+4.8\left(\frac{a}{W}-0.5\right)^2\right] \quad (3.6)$$

where (t) was the measured physical time and (t') was a modified time which compensated for variations of the initial crack length in the range 0.45<a/W<0.55. The specified crack lengths were a_m was machined notch depth, a_0 was the length of fatigue precrack and a was the total crack length (a_m+ a_0) as shown in Figure 3.8.

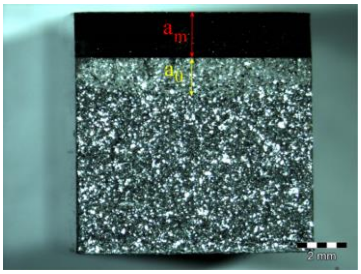

Figure 3.8 The fracture surface of the SENB specimen and specified crack lengths

4. Results and Discussion

4.1. Structural Characterization of Tested Steels

The microstructures of S355 steel in the longitudinal rolling direction were characterized by optical microscopy, as can be seen in Figure 4.1. It was visible that typical ferrites and pearlites were apparent. The dark regions refer to pearlite whereas light-colored regions refer to ferrite.

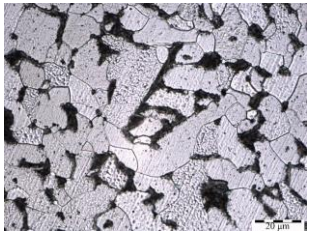

Figure 4.1 The microstructures of S355 steel (1000x)

The microstructural observation of Strenx 700MC steel sample is shown in Figure 4.2 (on the left). It was characterized by a fine-grained microstructure. The main heterogeneity of Strenx 700MC steel was carbide distribution as shown in Figure 4.2 (on the right). This heterogeneity affected the fracture response of the material which was explained in the following chapters.

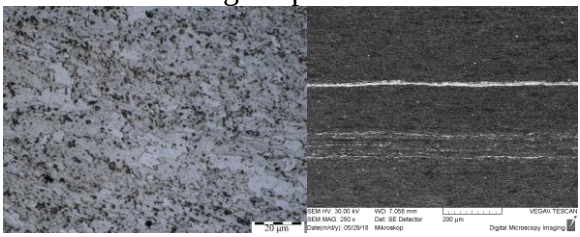

Figure 4.2 The microstructures of Strenx 700MC steel (left, 1000x) and the carbide distribution in Strenx 700MC (right)

4.2. Analyzes of the Welding Process Influence

4.2.1. Metallography Evaluation

Complex structural characterization of the experimental welding was conducted to:

- Identify the critical sublayer of HAZ in terms of structural degradation
- Describe the involved degradation process
- Enable suitable simulation process of welding influence.

The cross-sectional macro photo and microstructure of Strenx 700MC weld joints are displayed in Figure 4.3. The first noticeable observation in macrographs which is in the middle of Figure 4.3, macro porosities were observed in the welding pool. These defects confirmed that the weld thermal simulation was a better approach than real welding method for investigating the effect of heat input on the tested steel. Four regions with significant influence on fracture resistance were visible in macrograph: welding pool, grain coarsening zone, grain refinement zone and base metal. In the welding pool, during weld metal solidification, grains tend to grow in the direction of maximum heat extraction. A typical columnar shape of grains in the welding pool is shown in the upper position of Figure 4.3. Next to the welding pool, grain coarsening is visible compared to the zone of base metal. The high cooling rate and large grain size stimulate the ferrite to form side plates from the grain boundaries. In the lower position of Figure 4.3, the zone of grain refinement is presented. Observed intensity of grain size refinement was an effective strengthening mechanism. Finally, a rolling effect was visible in the zone of base material. Irregular, locally rough inclusions were observed.

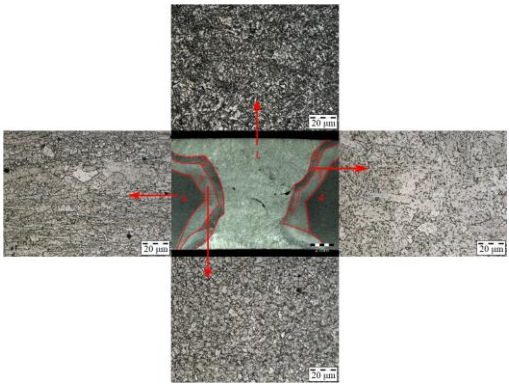

Figure 4.3 The cross-sectional macro photo and microstructures of Strenx 700MC weld joints, 1) welding pool, 2) grain coarsening zone, 3) grain refinement zone and 4) base metal

The structural evaluation was also conducted with scanning electron microscopy as shown in Figure 4.4. The microstructure of uninfluenced metal consisted of a fine-grained polygonal ferrite with a limited amount of pearlite. An increased heat input resulted in a broader coarse-grained zone. Primary grain morphology (Figure 4.4a) was not completely polygonal and effect of deformation during rolling was essentially maintained. The same effect was the reason for the lamellar morphology of fracture response during mechanical testing. The secondary phases dissolution was found as the most effective degradation process. It was followed by reprecipitation which led to the creation of reduced count and increased size mainly carbides (Figure 4.4c), hence the final effect in terms of mechanical behavior was measured as a significant decrease of hardness. An increased heat input in the zone adjacent to the fusion line resulted in a broader coarse-grained zone (Figure 4.4b).

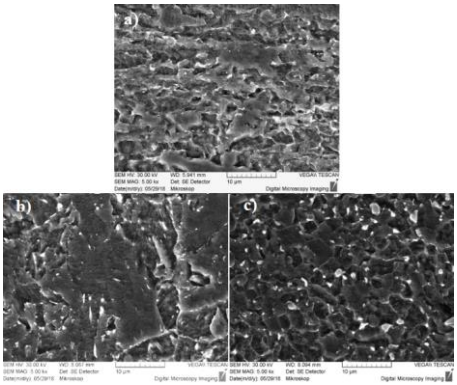

Figure 4.4 a) Uninfluenced steel, b) Fusion zone and c) Over A_3 of welded Strenx 700MC steel

4.2.2. Hardness Test Result of Welded Strenx 700MC

The exact positions and hardness values of the welded specimen are shown in Figure 4.5. Hardness values vs. distance from weld center is also plotted in Figure 4.6. The hardness value of the received base metal was approximately 295 HV1. In the region of the grain refinement zone, the hardness values varied from 245 HV1 to 266 HV1. Some sharp peaks were observed in the region between grain refinement and grain coarsening zone. The reason of high hardness value could be heterogeneity of the heat affected zone or small inclusions. The hardness measurement indicated that the lowest value in the sublayer of the outer part of the grain refinement zone (236 HV1). This result seemed to be in contradiction with generally known grain refining effect. Based on detail microstructure evaluation, it could be concluded that it was a result of partially austenitization process, together with lost both of primary strengthening processes – dislocation hardening and precipitation hardening. The latter one was more effective hence the reprecipitation of carbides has led to a substantial decrease of hardness. This value (236 HV1) had great importance because parameters of the weld thermal cycle simulation (maximum temperatures, heating and cooling time) were specified according to lowest hardness value. In the region of grain coarsening was very narrow and the hardness values were changing from 259 HV1 to 272 HV1. Common effect of grain coarsening – i.e. the decreasing of hardness, was overcome by

partial transformation to acicular ferrite and bainite. The welding pool had almost stable hardness value which was approximately 258 HV1.

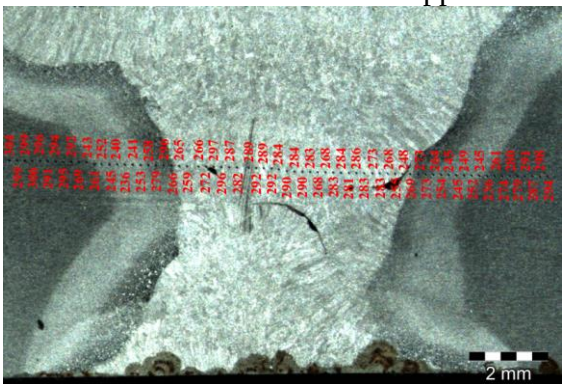

Figure 4.5 HV1 hardness survey across the cross-section of the welded Strenx 700MC

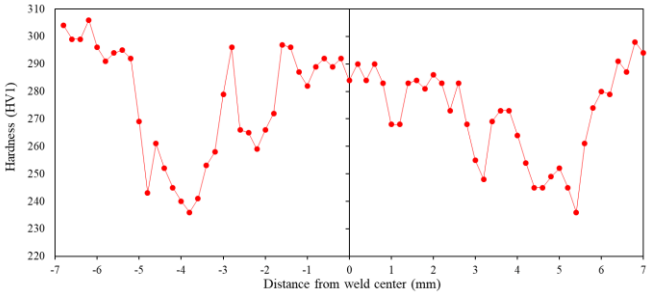

Figure 4.6 HV1 hardness vs. distance from weld center for welded Strenx 700MC specimen

4.3. Simulation of Welding Degradation Process

During the thermal cycle simulation, the specimen was rapidly heated to a maximum temperature of 800°C and held at this temperature for 5 seconds, the temperature was recorded as a function of time as shown in Figure 4.7.

The microstructure of the sample which was subjected to thermal cycle simulation is shown in Figure 4.8a. In the microstructure, side plate ferrite which is also called Widmanstatten ferrite was formed. Acicular ferrite was also formed because at lower temperatures it was too slow for Widmanstatten ferrite to grow into the grain interior. The acicular ferrite is desirable because it improves toughness of the metal. Based on results of metallography evaluation of the real welding influence, the carbide reprecipitation process was

found out as the most effective degradation process. In terms of that, the dissolution and recreation of carbides was also important validation of performed simulation process. As shown in Figure 4.8b, coarsening of the primary carbides was induced. This observation was in required accordance with the previous structural analyses results of real welding joints.

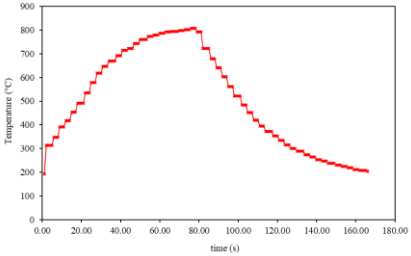

Figure 4.7 Weld thermal cycle profile for Strenx 700MC specimen

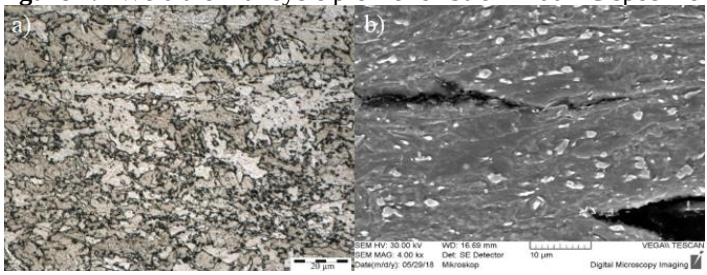

Figure 4.8 a) Microstructure and b) SEM image of Strenx 700MC specimen subjected to thermal cycle simulation

Hardness measurements were also performed on the sample which was subjected to weld thermal cycle simulation as shown in Figure 4.9. Almost stabile values in all cross section presented very important result in terms of simulation. It enabled to evaluate the change of fracture behaviour using both parameters – the fracture toughness and also the crack propagation resistance. Figure 4.10 shows the hardness vs. distance from notch to notch of the Strenx 700MC specimen subjected thermal cycle simulation. The hardness values of this specimen varied from 216 HV1 to 233 HV1 and mean value was approximately 225 HV1. As mentioned above, the main aim was approaching the lowest value (236 HV1) which was observed in the real welding sample of Strenx 700MC. In this way, it was possible to make an appropriate evaluation between real welding method and weld thermal cycle simulation.

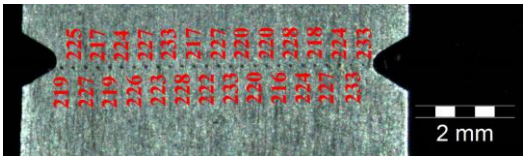

Figure 4.9 HV1 hardness survey across the cross-section of the Strenx 700MC specimen subjected to weld thermal cycle simulation

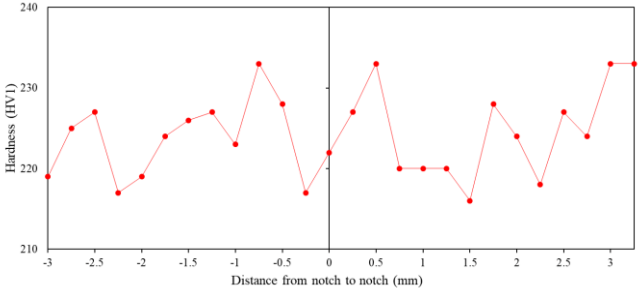

Figure 4.10 HV1 hardness vs. distance from notch to notch of Strenx 700MC specimen subjected to weld thermal cycle simulation

4.4. Result of CCRB Test Method

K_{IC} of S355 steel was tested for two different unnotched (D) and notched (d) diameters with constant D/d ratio as 1.2 to investigate the effect of diameters on fracture toughness. Strenx 700MC steel was selected to observe the effect of heat input which was conducted by weld thermal cycle simulation on fracture toughness. The fracture toughness values which were calculated using Equation 3.2 were tabulated in Table 4.1. In the table, the marking of S355 steel, experimental high strength steel, Strenx 700MC steel specimen and Strenx 700MC specimen which was subjected to weld thermal simulation were denoted as SCCRB, ECCRB, StxCCRB and StxWSCCRB, respectively (The figure of the cross-sectional and side view of the fractured all samples are given in Appendix B).

When the results of the fracture toughness values were evaluated for S355 steel, it can be seen from the data in Table 4.1, the diameter of the unnotched and notched sections had a significant effect on fracture toughness even if (D/d) ratio was kept constant as 1.2. For higher diameter, the fracture toughness of S355 steel varied from 35.78 MPa√m to 40.44 MPa√m and for lower diameter it varied from 51.01 MPa√m to 54.92 MPa√m. These results showed that as the

unnotched diameter along with notch diameter increased, the fracture toughness values decreased

The fracture toughness of Strenx 700MC steel were found to be highest value with using CCRB test methodology. It was expected result because it had fine grain microstructure and gave better resistance to crack propagation due to higher grain boundary area per unit volume. In the microstructure, grain boundary acted as a barrier to the crack growth mechanism. The fracture toughness of received Strenx 700MC steel specimen was found to be slightly higher than that of the specimen which was exposed to weld thermal cycle simulation. K_{IC} value was found to be in a range of 54.54 MPa√m to 58.21 MPa√m for received Strenx 700MC steel whereas it varied from 50.78 MPa√m to 52.32 MPa√m for same material after weld thermal cycle simulation. This difference can be explained on the basis of microstructures. The microstructure of Strenx 700MC specimen subjected to thermal cycle simulation was a combination of acicular and Widmanstatten ferrite whose grain size was slightly larger than that of heat untreated steel. The suppression of the heterogeneity after weld simulation process can be a second reason for decreasing in K_{IC} value.

Table 4.1 Fracture toughness values (K_{IC}) of the tested materials

Sample No	P_f (N)	D (mm)	a_m (mm)	a_f (mm)	d_{eff} (mm)	d_{eff}/D	K_{IC} (MPa√m)
SCCRB-01	51433	11.72	0.99	0.18	9.36	0.80	35.78
SCCRB-02	47644	11.80	0.98	0.50	8.84	0.75	38.13
SCCRB-03	46603	11.85	0.99	0.67	8.53	0.72	40.44
SCCRB-04	27284	7.77	0.76	0.50	5.24	0.67	51.01
SCCRB-05	24250	7.89	0.72	0.75	4.93	0.63	51.23
SCCRB-06	17957	8.05	0.75	1.28	3.98	0.49	54.92
ECCRB-01	20028	7.79	0.71	0.47	5.45	0.70	34.62
ECCRB-02	19931	7.72	0.71	0.45	5.40	0.70	34.94
ECCRB-03	22147	8.28	0.77	0.42	5.90	0.71	33.62
StxCCRB-01	28744	7.70	0.70	0.64	5.02	0.65	58.21
StxCCRB-02	31953	7.65	0.69	0.47	5.32	0.70	57.46
StxCCRB-03	32243	7.61	0.69	0.38	5.47	0.72	54.54
StxWSCCRB-01	34183	7.67	0.73	0.21	5.78	0.75	51.52
StxWSCCRB-02	24784	6.98	0.74	0.35	4.80	0.69	52.32
StxWSCCRB-03	24972	7.26	0.73	0.43	4.94	0.68	50.78

* (P_f) fracture load, (D) diameter of unnotched section, (a_m) machined notch depth, (a_f) length of fatigue precrack, (d_{eff}) effective diameter, (K_{IC}) fracture toughness

The lowest fracture toughness value was obtained for experimental high strength steel. It did not exhibit a significant amount of plasticity. The mean value of fracture toughness was obtained as 34.39 MPa√m for experimental high strength steel.

This study showed a correlation between d_{eff}/D ratio and K_{IC} value. It can be clearly seen in Figure 4.11, as the d_{eff}/D ratio increased, the fracture toughness value decreased. These observations were in agreement with the study of Neelakantha et al [28]. In that study, the valid range of Equation 3.2 was $0.46<(d_{eff}/D)<0.86$. This wide interval caused variations for calculation of fracture toughness values with using CCRB test methodology. In order to prevent the variations in fracture toughness value, this proposed interval limit can be reduced to lower values.

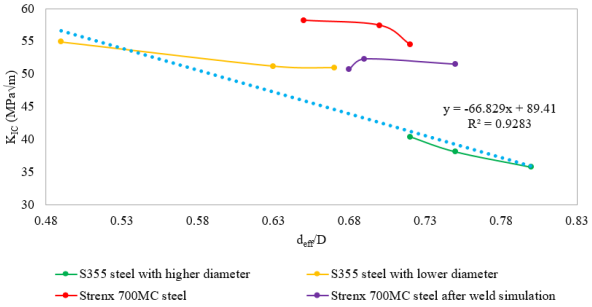

Figure 4.11 Correlation between d_{eff}/D and K_{IC} value

According to Nath and Das, the fracture toughness value of medium carbon steel was found to be 50 MPa√m, low carbon steel was found to be 25 MPa√m in the literature [29]. It was also reported that plane strain fracture toughness values of low carbon steels were in the range of 41 MPa√m to 82 MPa√m [30]. The used comparison was too general and it was necessary to accept the effect of notch sharpness, the constraint factor as a substance of the fracture mechanics approach. The reasons of the high difference value of K_{IC} depend on the production method and the heat treatment process. Bozkurt and Schmidová reported that as the notch angle increased, the value of the fracture toughness increased [31]. The similar tendency of increasing K_{IC} value as the notch increases was observed by Bayram et al. [32]. The reason of this observation was attributable to as the notch angle decreases, the triaxiality of stresses at the notch root increased and plastic deformation was increasingly suppressed. In this study, the obtained values were in the range of K_{IC} values reported in the literature.

4.5. Result of Dynamic Fracture Toughness with Nonstandardized Test Methods

In order to specify the maximum value of P_{dmax}, considering the first peak of the filtered force – displacement curve was fitted by using "curve fitting tool" in MS Office Excel software as shown in Figure 4.12. All results are tabulated in Table 4.2 and the marking of S355 and Strenx 700MC steel for higher and lower speed impact tensile tests were denoted as "S355D", "S355LSD", "StxD" and "StxLSD" respectively and experimental high strength steel were denoted as "ED". Lastly, Strenx 700MC specimen which was

subjected to weld thermal simulation was denoted as “StxWSD” (The figure of the cross-sectional and side view of the fractured all samples are given in Appendix C and the force – displacement graph of all tested steels is given in Appendix D).

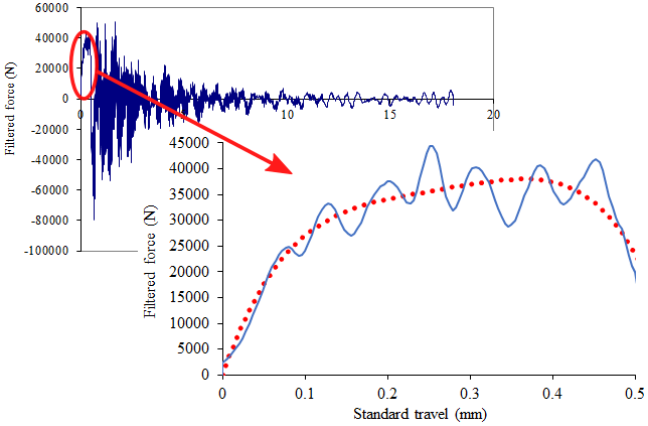

Figure 4.12 Curve fitted plot of force – displacement graph

Table 4.2 Dynamic fracture toughness values of tested all steels

Sample No	P_{dmax} (N)	D (mm)	a_m (mm)	a_f (mm)	d_{eff} (mm)	d_{eff}/D	K_{Id} (MPa√m)
S355D-01	38012	7.65	0.72	0.625	4.96	0.65	78.56
S355D-02	38032	7.77	0.73	0.72	4.87	0.63	81.86
S355D-03	37988	7.57	0.745	0.49	5.1	0.67	74.00
S355D-04	36756	7.79	0.735	0.99	4.34	0.56	97.15
S355D-05	35649	7.59	0.785	0.63	4.76	0.63	79.39
S355D-06	35389	7.76	0.72	0.81	4.70	0.61	81.27
S355D-07	30446	7.80	0.715	1.26	3.85	0.49	97.88
S355D-08	34854	7.79	0.735	1.03	4.26	0.55	95.06
S355LSD-01	35879	8.13	0.765	0.81	4.98	0.61	75.27
S355LSD-02	33794	8.23	0.745	0.88	4.98	0.61	71.18
S355LSD-03	32284	8.19	0.78	1.00	4.63	0.57	77.21
StxD-01	41484	7.59	0.695	0.32	5.56	0.73	67.71
StxD-02	40534	7.78	0.66	0.38	5.70	0.73	63.65
StxD-04	43833	6.95	0.535	0.21	5.46	0.79	69.61
StxD-05	38764	7.84	0.725	0.49	5.42	0.69	68.09
StxD-08	43510	7.80	0.72	0.49	5.38	0.69	77.29
StxLSD-01	43676	7.62	0.69	0.20	5.84	0.77	63.97
StxLSD-02	41164	8.11	0.75	0.42	5.77	0.71	64.68
StxLSD-03	44534	8.11	0.73	0.25	6.15	0.76	60.86
StxWSD-01	36057	7.22	0.83	0.45	4.66	0.65	81.98
StxWSD-02	22769	7.74	0.805	1.68	2.77	0.36	118.24
StxWSD-03	32839	7.20	0.575	0.67	4.71	0.65	73.06
ED-01	30694	7.76	0.725	0.68	4.95	0.64	64.05
ED-02	31853	7.82	0.75	0.57	5.18	0.66	61.11
ED-03	33836	7.89	0.75	0.51	5.37	0.68	60.69

* (P_f) fracture load, (D) diameter of unnotched section, (a_m) machined notch depth, (a_f) length of fatigue precrack, (d_{eff}) effective diameter, (K_{Id}) dynamic fracture toughness

For S355 steel, totally 8 specimens were tested at higher speed and 3 specimens were tested at lower speed in order to ensure reliability and repeatability of this test methodology. The first notable result was the plot of force – displacement curve had lots of vibrations during the impact event. But these vibrations did not existed when the

impact tensile was conducted with lower speed (from Figure D1 to Figure D11, in Appendix D) and generally exhibited a smooth curve for considering the first peak. As can be seen from the table (above), the fracture toughness values varied between 74 MPa√m and 97.88 MPa√m. The first reason for this high interval could be during the impact tensile test, existing of large amplitudes in force – displacement graphs. It was mathematically evident that large vibrations were resulted with higher dynamic fracture toughness value for S355D-04, S355D-07 and S355D-08 specimens. The second reason for higher K_{Id} value was a correlation between d_{eff} and dynamic fracture toughness. It can be clearly seen from the table, as the d_{eff} decreased, K_{Id} value increased and the same behaviour was also seen while calculating the plane strain fracture toughness (K_{IC}) of S355 steel. The K_{Id} values of the rest samples were in range from 74 MPa√m to 81.86 MPa√m. A comparison of higher and lower speed impact tensile test revealed that S355 steel was typically sensitive to the loading rate. With the speed of pendulum decreased from 5.23 m/s to 3.48 m/s, the value of dynamic fracture toughness decreased approximately 12% for the calculated mean value. As the K_{Id} value was calculated with Equation 3.3, higher loading rate did not allow time for stress redistribution and it was resulted with higher maximum dynamic force (P_{dmax}). Generally, by increasing strain rate, the yield strength and tensile strength of the steels increase. But this strain hardening process, some of the steels are strongly depended while some of the steels has less strain sensitivity.

For Strenx 700MC steel, at higher pendulum speed totally 8 and at lower speed totally 3 of impact tensile test was conducted. During the fatigue precracking procedure, even though the same bending moment and number of cycle was applied to all specimen, StxD-03, StxD-06 and StxD-07 specimens were not fractured from the cross-sectional alignment of the notched section. Because of this reason, the dynamic fracture toughness values of the mentioned specimens could not be calculated. The side view of these specimens is shown in Figure C14, Figure C17 and Figure C18 in Appendix C. They had unique fracture appearance in terms of fracture mechanics. Half part of the specimen had one macro hill and the other part of the

specimen had macro valley and tearing of the specimen was also observed. Considering force – displacement graphs which are given in Appendix D (Figure D3, Figure D6, Figure D7) gradual response is the supporting of the unique fracture appearance. The possible reason of this behavior, the material heterogeneity which was caused by the manufacturing process was more dominant than fatigue precracking. From the cross-sectional view of all fractured specimens (in Appendix C), length of fatigue precrack was not propagated equidistantly. As can be seen from the figures, the crack was not initiated in some points from machined notch tip and it was resulted with one side or nonhomogeneous crack propagation. The calculated dynamic fracture toughness for higher loading rate varied between 63.65 MPa√m and 77.29 MPa√m, and for lower loading rate in the range from 60.86 MPa√m to 64.68 MPa√m. Considering the calculated mean values, K_{Id} values of the lower loading rate decreased approximately 8% in comparison to a higher loading rate. These results showed that Strenx 700MC steel less sensitive than S355 steel. The response of the force – displacement graph was smoother, and less vibration was observed during the impact tensile test. After conducting the weld thermal cycle simulation, the value of the calculated dynamic fracture toughness increased but ratio of d_{eff}/D was not in valid range which was suggested as $0.46<(d_{eff}/D)<0.86$ for only StxWSD-02 specimen. One interesting finding was the length of fatigue precrack was propagated almost in equidistantly and the crack was initiated along every point of the circumferential machined notch tip. After weld thermal cycle simulation process, almost flat surface was observed instead of the macro hill and valley. With heat supplying to the specimens, they have gained resistance to crack propagation and it exhibited higher dynamic fracture toughness value in comparison to the non-heat-treated specimens.

The experimental high strength steel specimens were tested only at 5.23 m/s pendulum speed. The lowest value was obtained for dynamic fracture toughness K_{Id} value as well as for the plane strain fracture toughness K_{IC} value. Taking into account with the mean value of K_{Id} was higher approximately 44% that of K_{IC}. This percentage value was 38% for S355 steel and 18% for Strenx 700MC steel. It was

apparent that the experimental high strength steel was the most sensitive for the loading rate among the examined all specimen. The characteristic of force – displacement graph had very sharp peak, but less oscillation was observed for the first peak. The cross-sectional view of the fractured specimens had shiny appearance which was the proof of brittle fracture mechanism and the side view was completely flat. These findings were supported by having the lowest value of experimental high strength steel.

4.6. Validation of Novel Methodology

4.6.1. Result of Dynamic Fracture Toughness with Standardized Test Methods

Experimental high strength steel was chosen as referential steel for validation of novel methodology. Low initial plasticity enables to apply the limited dimensions of tested samples, i.e. comparative with CCRB method. The force – time plots are given in Appendix E and the measured crack lengths are given in Appendix F.

The defined dimensions, time to fracture and calculated dynamic fracture toughness values are tabulated in Table 4.3. The results of K_{Id} values obtained by the standardized test method were consistent with that of the nonstandardized test method. It has to be mentioned that ratio of (a/W) is not in valid range which is suggested as ($0.45<a/W<0.55$) by ISO standard. Despite this possible influence, very close results were obtained (the calculated mean value of standard method was 56.69 MPa√m while that of nonstandardized method was 61.95 MPa√m). In conclusion, the novel method provides the possibility of acquiring the dynamic fracture toughness for metallic materials.

Table 4.3 Calculated dynamic fracture toughness value according to ISO 26843:2015(E)

Sample No	a (mm)	W (mm)	a/W	t' (μs)	f(t) (μs)	K_{Id} (MPa√m)
ESD-01	3.18	9.82	0.32	21.36	35.43	55.77
ESD-02	3.29	9.84	0.33	25.94	38.98	61.36
ESD-03	4.07	9.62	0.42	22.89	33.63	52.94

4.6.2. Fracture Analysis of Experimental High Strength Steel

SEM image of ECCRB-02 experimental high strength steel specimen which was fatigue precracked and following static tensile

loaded is shown in Figure 4.13. According to K_{IC} results, the experimental high strength steel had the lowest fracture toughness values in comparison to other tested steels. In the zone of sudden unstable fracture mode was completely brittle fracture and the cleavages were visible. These findings confirmed that the experimental high strength steel specimen had lowest K_{IC} value.

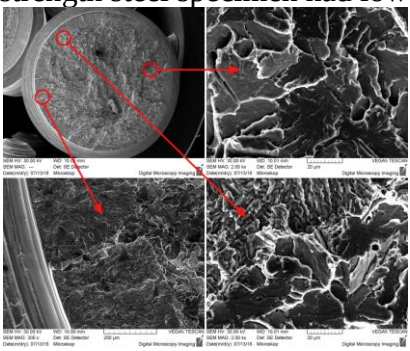

Figure 4.13 SEM image of ECCRB-02 specimen

SEM image of ED-01 experimental high strength steel specimen which was fatigue precracked and following impact tensile loaded is shown in Figure 4.14. It had almost same fracture surface with ECCRB-02 specimen.

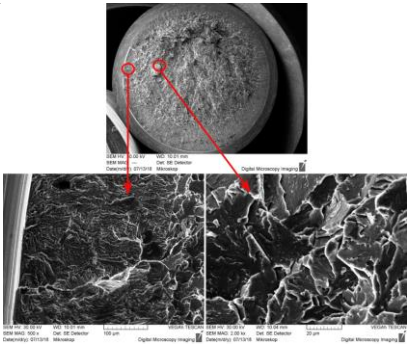

Figure 4.14 SEM image of ED-01 specimen

4.7. Influence of Loading Rate on Fracture Response

Sensitivity of compared steels on inner imperfections and passive safety capacity can be evaluated by detail examination SEM analysis of fractured specimens. The novel method was also applied for comprehensive study of every stage of crack propagation, as a

tracing of prospective inner defect influence during different operational loading.

4.7.1. Standard Steel

The fractured surface of the SCCRB-05 specimen which was fatigue precracked and following static tensile loaded is given in Figure 4.15. It can be clearly seen in macroscopic scale that there are two distinct regions were existed. The first region was crack propagation zone and the macro beach marks were visible. The fatigue crack was propagated in equal distance from the machined notch tip and no eccentricity was observed through circumferential direction. The second region was the result of the static tensile loading and it was distinctive in comparison to the crack propagation zone. This zone exhibited two different characteristics. The initial moment of the static tensile loading, fracture surface displayed undulating appearance. A number of small and big cup like depressions were observed in the fractographs. This depression were generally known as dimples. The cup like depressions shows that the material exhibits ductile fracture mechanism. In the final stage of the static tensile loading, the fracture mechanism was changed from ductile to brittle fracture type. It can be clearly seen from the figure (lower-right) final unstable part has cleavage type which is the proof of the brittle fracture mechanism.

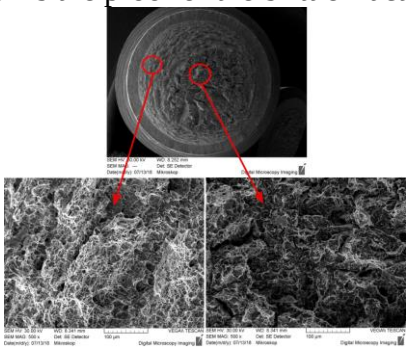

Figure 4.15 SEM image of SCCRB-05 specimen

The fractured surface of the S355D-02 specimen which was fatigue precracked and following impact tensile loaded at pendulum speed 5.23 m/s is given in Figure 4.16. The overall sectional view of the fatigue fractured surface showed smooth surface finish. In comparison to SCCRB-05 specimen, the distance of undulating

appearance (uphill and downhill steps) was narrower. The possible reason of this observation was higher loading rate. Higher strain rate did not allow time for stress redistribution and it promoted the brittle fracture type.

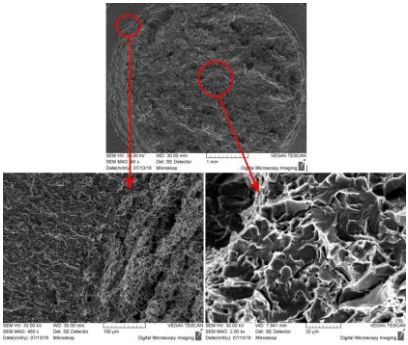

Figure 4.16 SEM image of S355D-02 specimen

The fractured surface of the S355LSD-02 specimen which was fatigue precracked and following impact tensile loaded at pendulum speed 3.48 m/s is given in Figure 4.17. The same fracture characteristics were observed with S355D-02 specimen

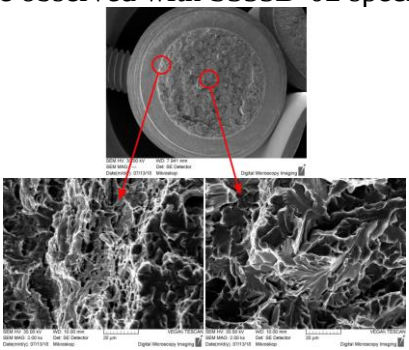

Figure 4.17 SEM image of S355LSD-02 specimen

Representative force – displacement graph is shown in Figure 4.18. S355 steel displayed an increase in fracture load with increasing loading rate. This was expected because mechanisms which easily move dislocations under low loading rates were deactivated at higher loading rates. The obtained result was consistent with the findings of previous works [33–36]. Boyce and Dilmore reported that the increase in strength with increasing strain rate is typically attributed to the reduction of diffusion limited (thermal) dislocation processes to

overcome short range obstacles [33]. Increasing fracture load led to an increase in the static (K_{IC}) and the dynamic (K_{Id}) fracture toughness because of they were directly proportional to the fracture loads.

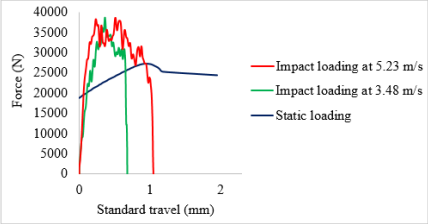

Figure 4.18 Force-displacement graph of S355 specimen at different loading rate

4.7.2. Prospective High Strength Steel

In Figure 4.19, fractographs of StxCCRB-01 specimen which was fatigue precracked and following static tensile test is performed is shown. In comparison to other tested steels, it was visible that the length of fatigue crack propagation was completely heterogeneous. It started from the tip of the machined notch, but it was not propagated equally through in circumferential direction. In the middle of the broken specimen, sharp micro hills were observed. These micro hills were existed because of the steel had internal heterogeneity. In the region of static tensile loading, the fracture mode was mixed mode. In some region, cleavage was existed and in the rest of the fractured surface, microvoid coalescence was observed.

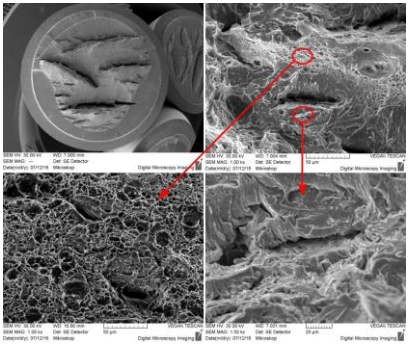

Figure 4.19 SEM image of StxCCRB-01 specimen

The SEM fractured surfaces of StxD-05 specimen and StxLSD-01 specimen are shown in Figure 4.20 and in Figure 4.21, respectively. Between two different loading conditions, the region of fatigue precracking and unstable fracture were almost same. Both of

them had mixed-mode ductile and brittle cracking mechanism. The most noticeable difference was the appearance of the micro hills. A large number of micro parallel hills were observed at higher pendulum speed whereas limited number of micro hills were existed at lower pendulum speed.

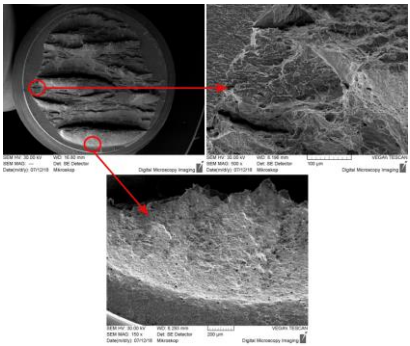

Figure 4.20 SEM image of StxD-05 specimen

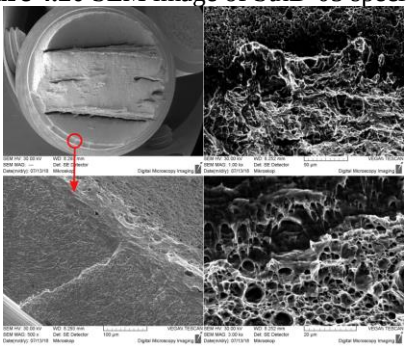

Figure 4.21 SEM image of StxLSD-01 specimen

Representative force displacement graph is shown in Figure 4.22. A similar trend which was seen in S355 steel was also observed for Strenx 700MC steel, the fracture load was increased with increasing loading rate.

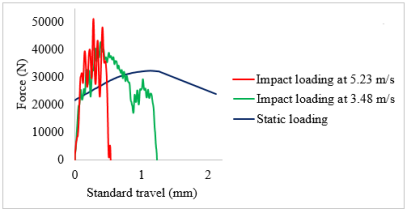

Figure 4.22 Force-displacement graph of Strenx 700MC specimen at different loading rate

4.8. Influence of Welding Process on Crack Sensitivity

The SEM fractured surfaces of StxWSCCRB-03 specimen and StxWSD-01 specimen are shown in Figure 4.23 and in Figure 4.24, respectively. In Figure 4.23, it can be clearly seen that after fatigue precracking region, two different fracture mechanisms were observed. Firstly, resulted in a typical microvoid coalescence morphology and ductile fracture mode as expected after weld thermal cycle simulation. There were subtle differences in terms of dimple size. Secondly, the microvolume of cleavages was observed which was the proof of brittle fracture mechanism. In Figure 4.24, (upper-left) fractured surface had radial marks which were macroscopic surface features that indicate the region of crack initiation and propagation direction and also this figure revealed that the notch was not machined properly. This machining defect was resulted with heterogeneous crack propagation through the circumferential direction. Representative force displacement graph is shown in Figure 4.25. The same behaviour was also observed after the weld thermal cycle simulation process. The fracture load increased by increasing loading rate.

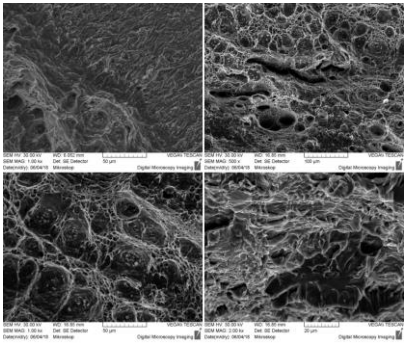

Figure 4.23 SEM image of StxWSCCRB-03 specimen

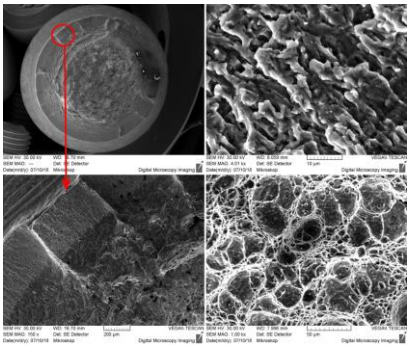

Figure 4.24 SEM image of StxWSD-01 specimen

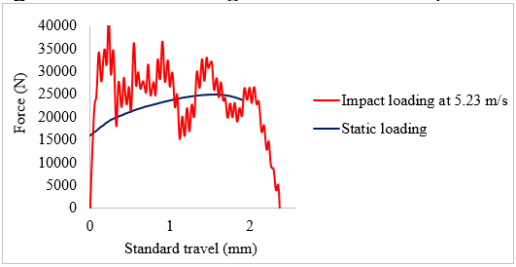

Figure 4.25 Force-displacement graph of Strenx 700MC specimen after weld thermal simulation

5. Conclusions

This experimental research study, using the standard and the novel methodology, provided a lot of particular information. The result obtained from this doctoral dissertation can be summarized as follows:

- To identify the degradation process, structural characterization of the experimental welding was conducted for Strenx 700MC steel and hardness measurements were performed. It indicated that the lowest value in sublayer of outer part of the grain refinement zone. It was in contradiction with generally known grain refining effect. Based on detail microstructure evaluation, it was observed that the reprecipitation of carbides has led to substantial decrease of hardness.
- The weld thermal cycle simulation was designed based on analyses of experimental welding process influence. Hardness measurement showed almost stabile values in all cross section. It enabled to evaluate the change of fracture behaviour using both parameters – the fracture toughness and also the crack propagation resistance.

- K_{IC} value of Strenx 700MC steel specimen was found to be slightly higher than that of the specimen which was exposed to weld thermal cycle simulation. Microstructure of Strenx 700MC specimen subjected to thermal cycle simulation was combination of acicular and Widmanstatten ferrite and the suppression of the heterogeneity after weld simulation process could be reasons for decreasing in K_{IC} value.
- After conducting the weld thermal cycle simulation, the value of the calculated dynamic fracture toughness increased in comparison to the heat untreated Strenx 700MC specimen. Contrary to expectations, the heat input did not induce the degradation of crack dynamic resistance of this high strength steel.
- The plane strain fracture toughness (K_{IC}) was determined with circumferentially notched round bar (CNRB) and circumferentially cracked round bar (CCRB) for S355, Strenx 700MC and experimental high strength steels. The highest K_{IC} value was obtained for Strenx 700MC steel, followed by S355 steel and experimental high strength steel.
- The difference of the calculated K_{IC} values between CNRB and CCRB methodologies was remarkable and it was investigated with fracture mechanics aspect. Fracture toughness determination of metallic materials with using these approaches was easy, reliable and accurate method.
- The diameter of the unnotched and notched sections had significant effect on fracture toughness even if (D/d) ratio was kept constant as 1.2. It was found that as the unnotched diameter along with notch diameter increased, the fracture toughness values were decreased.
- It was found a correlation between d_{eff}/D ratio and K_{IC} value. As the d_{eff}/D ratio increased, the fracture toughness value decreased.
- The new approach was used for evaluation of dynamic fracture toughness (K_{Id}) of metallic materials. Considering calculated mean dynamic fracture toughness, the highest (K_{Id}) value was obtained for S355 steel, followed by Strenx 700MC and experimental high strength steel. In higher loading rate, Strenx 700MC steel exhibited lower crack resistance in comparison to static loading conditions.
- Regardless of the grade of the steel, as the loading rate increased from 3.48 m/s to 5.23 m/s, calculated (K_{Id}) value increased for the

novel methodology. All of the tested steels induced some micro plasticity at the propagated crack tip.

- The novel method was compared with ISO 26843:2015(E) standard which uses single edge notch bend specimen. The obtained results showed that the calculated K_{Id} values were very close each other for experimental high strength steel.
- The SEM analysis supported the experimental results. Experimental high strength steel with the lowest fracture toughness values, displayed totally brittle cleavage cracking while S355 and Strenx 700MC steels exhibited almost mixed-mode ductile and brittle cracking mechanism in static and dynamic loading conditions. In all specimen, crack propagation zone was visible.

6. References

[1] I. Dincer, J. Hogerwaard, and C. Zamfirescu, 2015, Clean Rail Transportation Options, Springer Science+Business Media, New York, NY.

[2] A. Kurc-Lisiecka, J. Piwnik, and A. Lisiecki, 2017, "Laser Welding of New Grade of Advanced High Strength Steel STRENX 1100 MC," Arch. Metall. Mater., 62(3), pp. 1651–1657.

[3] R. Ulewicz, P. Szataniak, F. Novy, L. Trsko, and O. Bokuvka, 2017, "Fatigue Characteristics of Structural Steels in the Gigacycle Region of Loading," Mater. Today Proc., 4(5), pp. 5979–5984.

[4] J. Laitila, J. Larkiola, and D. Porter, 2018, "Effect of Forced Cooling on the Tensile Properties and Impact Toughness of the Coarse-Grained Heat-Affected Zone of a High-Strength Structural Steel," Weld. World, 62(1), pp. 79–85.

[5] M. Mazur, and R. Ulewicz, 2017, "Analysis of Strength and Fatigue Properties of Construction Materials for Manufacturing the Parts of Semi-Trailers," 2(1), pp. 32–37.

[6] R. Ulewicz, and P. Szataniak, 2016, "Fatigue Cracks of Strenx Steel," Mater. Today Proc., 3(4), pp. 1195–1198.

[7] J. Górka, 2015, "Weldability of Thermomechanically Treated Steels Having a High Yield Point," Arch. Metall. Mater., 60(1), pp. 469–475.

[8] M. Mazur, 2016, “Fatigue Properties of Fine-Grained Steels Applied in Components of Semitrailers,” Tech. Trans. Mech., 4M/2016, pp. 9–14.
[9] J. Górka, and S. Stano, 2018, “Microstructure and Properties of Hybrid Laser Arc Welded Joints (Laser Beam-MAG) in Thermo-Mechanical Control Processed S700MC Steel,” Metals, 8(2), pp. 132–147.
[10] J. Sperle, L. Hallberg, J. Larsson, and H. Groth, 2008, “The Environmental Value of High Strength Steel Structures", The Steel Eco-Cycle, Environmental Research Programme for the Swedish Steel Industry, 2004 – 2012, The Steel Eco-Cycle. Scientific Report. Phase 1, 2004 – 2008,” pp. 151–171.
[11] F. Bozkurt, 2015, “Structural and Mechanical Heterogeneities of Fine Grain Steel Welded Joints Used in Construction of Rail Vehicles,” Master Thesis, 96 p., University of Pardubice.
[12] K. Weman, 2012, Welding Processes Handbook, Woodhead Pub, Oxford ; Philadelphia.
[13] Md. I. Khan, 2007, Welding Science and Technology, New Age International (P) Ltd., Publishers, New Delhi.
[14] S. Kou, 2003, Welding Metallurgy, Wiley-Interscience, Hoboken, N.J.
[15] S. Kim, D. Kang, T. Kim, J. Lee, and C. Lee, 2011, “Fatigue Crack Growth Behavior of the Simulated HAZ of 800MPa Grade High-Performance Steel,” Mater. Sci. Eng. A, 528(6), pp. 2331–2338.
[16] W. Liu, F. Lu, R. Yang, X. Tang, and H. Cui, 2015, “Gleeble Simulation of the HAZ in Inconel 617 Welding,” J. Mater. Process. Technol., 225, pp. 221–228.
[17] J. Górka, 2012, “An Influence of Welding Thermal Cycles on Properties and HAZ Structure of S700MC Steel Treated Using Thermomechanical Method,” pp. 41–44.
[18] S. Kumar, S.K. Nath, and V. Kumar, 2016, “Continuous Cooling Transformation Behavior in the Weld Coarse Grained Heat Affected Zone and Mechanical Properties of Nb-Microalloyed and HY85 Steels,” Mater. Des., 90, pp. 177–184.

[19] M. Dunđer, I. Samardžić, and Š. Klarić, 2007, "Influence of Cooling Time Δt8/5 on Welded Joint Properties of the Thermal Cycle Simulated TStE 420 Specimens," Teh. Vjesn., 14(1,2), pp. 47–57.
[20] Z. Boumerzoug, E. Raouache, and F. Delaunois, 2011, "Thermal Cycle Simulation of Welding Process in Low Carbon Steel," Mater. Sci. Eng. A, 530, pp. 191–195.
[21] Y. Shi, and Z. Han, 2008, "Effect of Weld Thermal Cycle on Microstructure and Fracture Toughness of Simulated Heat-Affected Zone for a 800MPa Grade High Strength Low Alloy Steel," J. Mater. Process. Technol., 207(1–3), pp. 30–39.
[22] X. Kong, and C. Qiu, 2013, "Continuous Cooling Bainite Transformation Characteristics of a Low Carbon Microalloyed Steel under the Simulated Welding Thermal Cycle Process," J. Mater. Sci. Technol., 29(5), pp. 446–450.
[23] W. Zhao, W. Wang, S. Chen, and J. Qu, 2011, "Effect of Simulated Welding Thermal Cycle on Microstructure and Mechanical Properties of X90 Pipeline Steel," Mater. Sci. Eng. A, 528(24), pp. 7417–7422.
[24] J. Winczek, and A. Kulawik, 2012, "Dilatometric and Hardness Analysis of C45 Steel Tempering with Different Heating-up Rates," Metalurgija, 51(1), pp. 9–12.
[25] T. Vuherer, M. Dunđer, L. Milović, M. Zrilić, and I. Samardžić, 2013, "Microstructural Investigation of the Heat-Affected Zone of Simulated Welded Joint of P91 Steel," Metalurgija, 52(3), pp. 317–320.
[26] I. Samardžić, A. Stoić, D. Kozak, I. Kladaric, and M. Dunđer, 2013, "Application of Weld Thermal Cycle Simulator in Manufacturing Engineering," Manuf. Ind. Eng., 12(1–2), pp. 7–11.
[27] I. Samardžić, A. Čikić, and M. Dunđer, 2013, "Accelerated Weldability Investigation of TStE 420 Steel by Weld Thermal Cycle Simulation," Metalurgija, 52(4), pp. 461–464.
[28] V.L. Neelakantha, T. Jayaraju, P. Naik, D. K. K, C.R. Rajashekar, and Mohankumar, 2015, "Determination of Fracture Toughness and Fatigue Crack Growth Rate Using Circumferentially Cracked Round Bar Specimens of Al2014T651," Aerosp. Sci. Technol., 47, pp. 92–97.

[29] S. Nath, and U. K. Das, 2008, “Effect of Microstructure and Notches on the Fracture Toughness of Medium Carbon Steel,” J. Nav. Archit. Mar. Eng., 3(1), pp. 15–22.
[30] Cambridge University Engineering Department, 2003, Materials Data Book.
[31] F. Bozkurt, and E. Schmidová, 2018, “Effect of Notch Angle on Fracture Toughness of AISI 4340 Using Circumferentially Notched Bars,” 27th Anniv. Int. Conf. Metall. Mater. Met. 2018.
[32] A. Bayram, A. Uğuz, and M. Ula, 1999, “Effects of Microstructure and Notches on the Mechanical Properties of Dual-Phase Steels,” Mater. Charact., 43(4), pp. 259–269.
[33] B.L. Boyce, and M.F. Dilmore, 2009, “The Dynamic Tensile Behavior of Tough, Ultrahigh-Strength Steels at Strain-Rates from $0.0002s^{-1}$ to $200s^{-1}$,” Int. J. Impact Eng., 36(2), pp. 263–271.
[34] A.R. Khalifeh, A.Dehghan Banaraki, H. Danesh Manesh, and M.Dehghan Banaraki, 2018, “Investigating of the Tensile Mechanical Properties of Structural Steels at High Strain Rates,” Mater. Sci. Eng. A, 712, pp. 232–239.
[35] N. Tsuchida, H. Masuda, Y. Harada, K. Fukaura, Y. Tomota, and K. Nagai, 2008, “Effect of Ferrite Grain Size on Tensile Deformation Behavior of a Ferrite-Cementite Low Carbon Steel,” Mater. Sci. Eng. A, 488(1–2), pp. 446–452.
[36] N.K. Singh, E. Cadoni, M.K. Singha, and N.K. Gupta, 2011, “Dynamic Tensile Behavior of Multi Phase High Yield Strength Steel,” Mater. Des., 32(10), pp. 5091–5098.